

가 (CT) (MRI)

, CT, MRI (1-3) 3-5 cm (thinning)
 , 2.6% (hyperostosis frontalis interna) 90%
 (4), 7% (wormian bones), (lacunar skull)
 가
 (Diploic space) 가 1 cm
 (base) (vault), 가
 (1). CT MRI
 T1 -
 (diploe) (venous lake)가
 (pacchionian granulation)가 가
 24
 (Epidermoid) (Dermoid cyst)
 가
 () 가
 (Fig. 1A, B).
 MRI (2).

1
2

(Fibrous dysplasia) (Fig. 2A, B). 20 가 . MRI T1 - T2 - (Albright) (1). (Hemangioma) 0.2% 3 (5). (scalloping) 가 가 (Eosinophilic granuloma) -X 3가 60% (beveled edge) 가 (sequestrum) (Fig. 4A, B). MRI T1 - (dural enhancement) (3).

(honeycombing) (trabecula) (Fig. 3B). MRI T1 - (Fig. 3C). 가

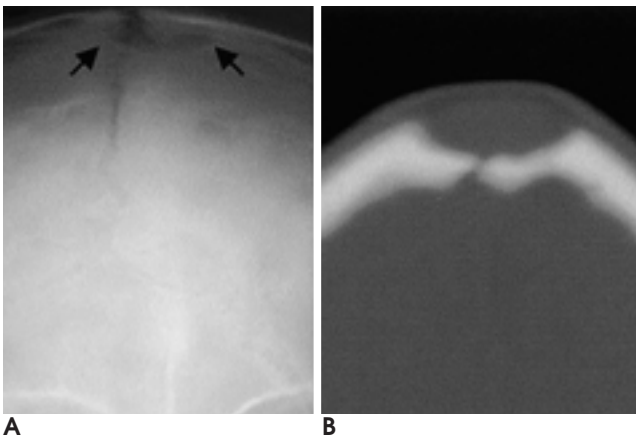


Fig. 1. A 4-year-old male with dermoid cyst.
A. Plain radiograph shows a well-defined lucent area and thin sclerotic rim (arrows).
B. Pre-enhanced CT scan shows a sharply defined osteolytic mass with thickening of outer tables at the margin of the lesion.

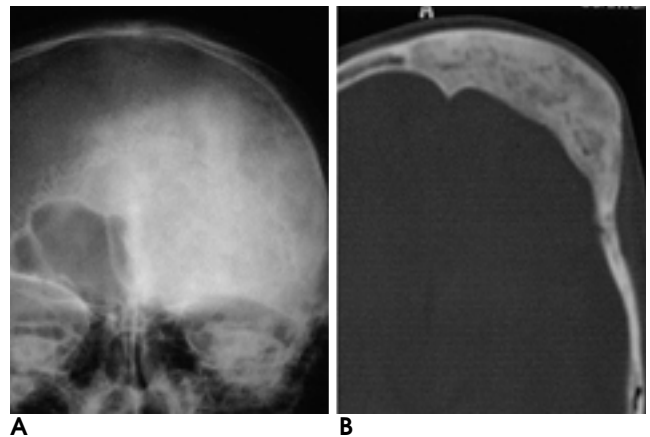


Fig. 2. A 19-year-old male with fibrous dysplasia.
A. Plain radiograph shows classic features of fibrous dysplasia including sclerosis in left frontal bone.
B. CT scan reveals osteoblastic appearance of left frontal bone and outward bulging.

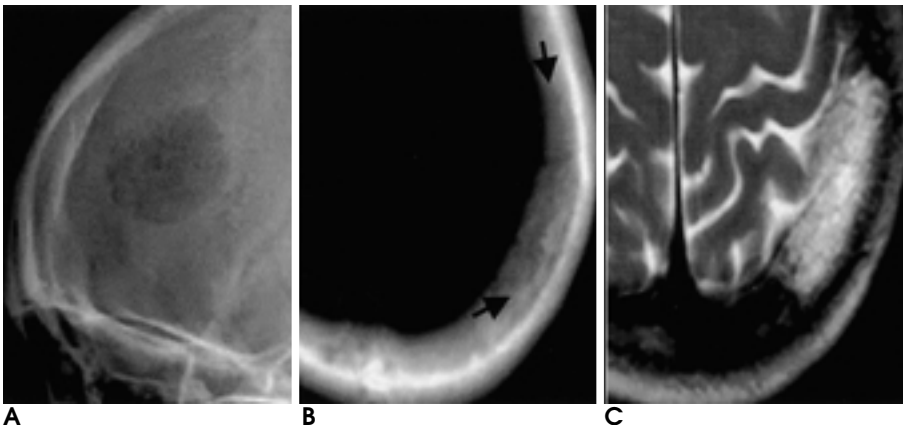


Fig. 3. A 37-year-old female with hemangioma.
A. Plain radiograph presents the granular, honeycomb appearance for hemangioma in left frontal bone.
B. Axial CT scan shows coarse trabeculated lesion in left parietal bone. The scalloped, nonsclerotic margins are clearly shown (arrows).
C. T2WI shows mesh-like high signal intensity that represents thickened trabeculation in mass.

(Osteoma)
 가 가 CT (Fig. 5A, B).
 가 (Gardner) MRI
 (1).
 가 (Meningioma)
 가 (osteoblastic activity)

가 (Fig. 6A).
 가 가 (psammoma body)가 CT 가
 가 MRI (3).
 (Fig. 6B).
 (Metastasis)
 가

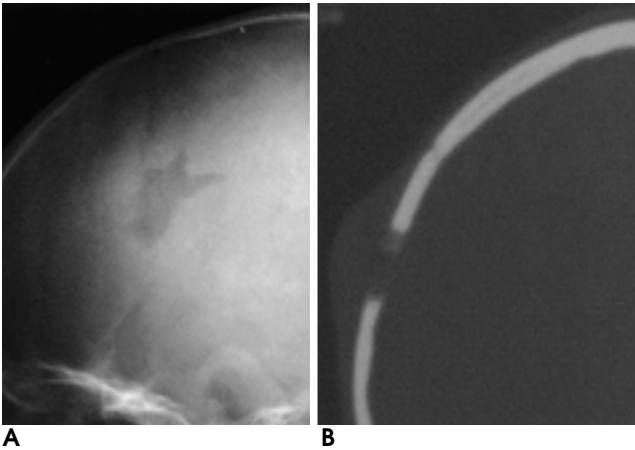


Fig. 4. A 5-year-old female with eosinophilic granuloma.
A. Plain radiograph shows well circumscribed lesion in right parietal bone of calvaria.
B. CT scan shows lytic, beveled lesion in right parietal bone. Button sequestrum is absent.

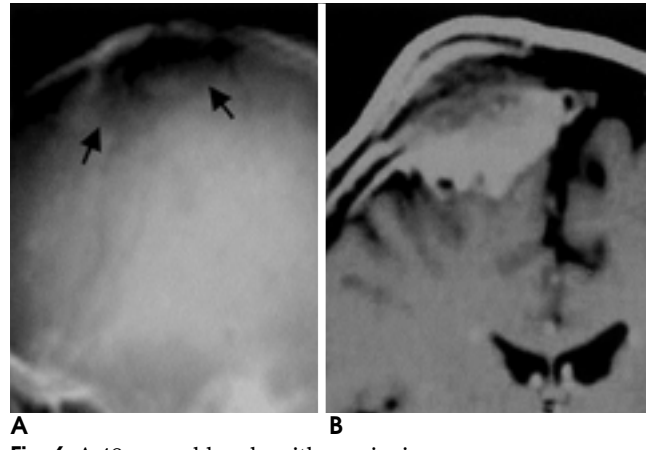


Fig. 6. A 49-year-old male with meningioma.
A. Plain radiograph shows purely lytic lesion with irregular margin and faint reticular or spiculated internal architecture in right parietal bone (arrows).
B. Coronal Gd-enhanced T1WI shows marked enhancement of tumor with intracranial and extracranial extension.

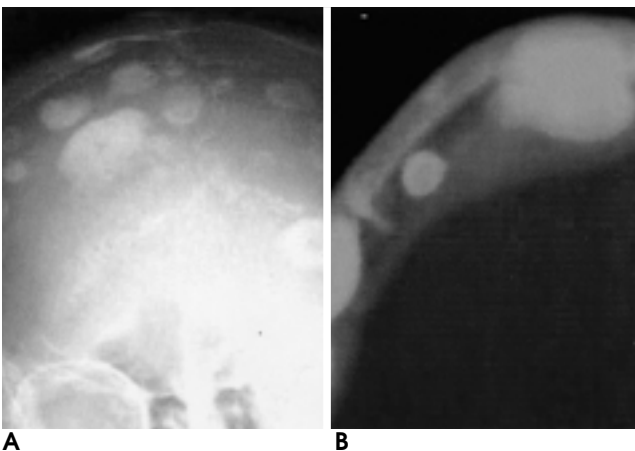


Fig. 5. A 15-year-old male with multiple osteomas.
A. Tangential view shows the flattened, varieties of osteomas arising from the inner table of the skull.
B. Axial CT scan shows multiple inner table osteomas with well-defined margin.

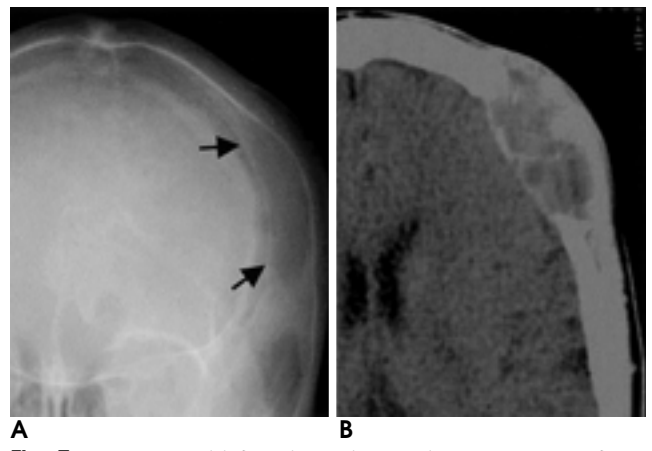


Fig. 7. A 55-year-old female with osteolytic metastasis from thyroid cancer.
A. Plain radiograph shows single irregular, ill-defined lucent area in left frontal bone (arrows).
B. Pre-enhanced CT scan shows osteolytic mass with bulging of inner and outer tables.

가
 (Fig. 7A, B).
 (Fig. 8) (1,
 ,가
 가
 (Ewing sarcoma) 10-25 75%가
 2%
 (onion skinning periosteal reaction)
 (Fig. 9). CT MRI 90%
 (8).
 8%

10
 5%
 (Codman)
 가
 (2).
 가
 (Neuroblastoma) , , 가
 (Fig. 10A,
 B). (2).
 (Osteosarcoma)
 가

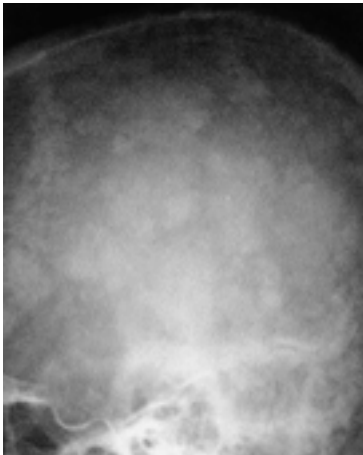


Fig. 8. A 65-year-old male with osteoblastic metastasis from prostatic carcinoma. Plain radiograph shows multiple increased densities outlined by lucency. Ill-defined lesions are seen throughout the skull.

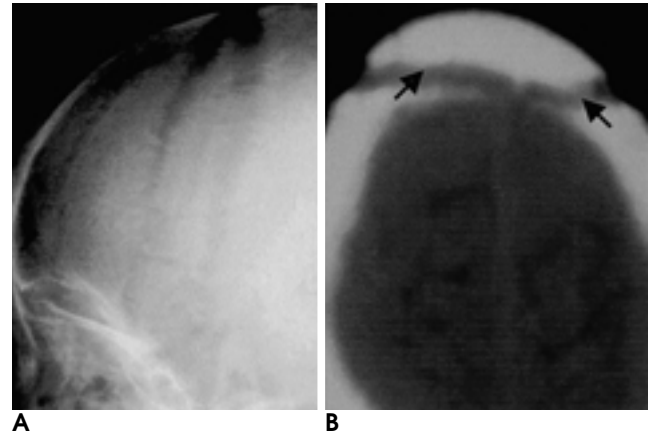


Fig. 10. A 3-year-old female with neuroblastoma. **A.** Plain radiograph shows widening of coronal suture. **B.** CT scan shows widened suture and spiculated margin of inner and outer tables (arrows). This represents metastatic tumor infiltration.

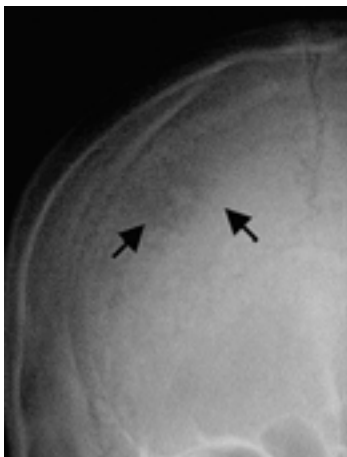


Fig. 9. A 19-year-old male with Ewing's sarcoma. Plain radiograph shows large lytic area with purely defined margin in right parietal bone (arrows). There is no periosteal reaction or thickening of the calvarium.

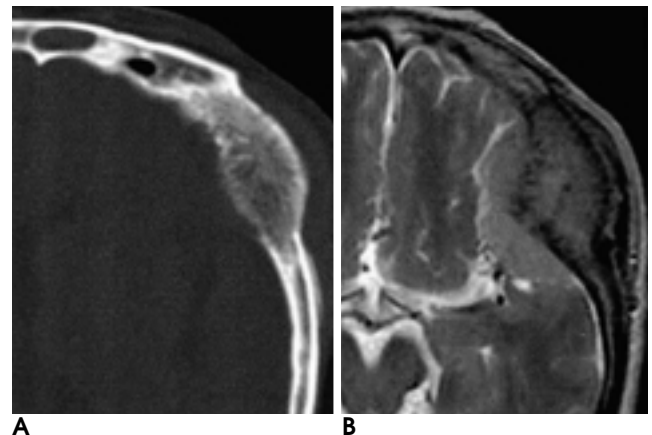


Fig. 11. A 30-year-old male with osteosarcoma. **A.** CT scan shows spiculated tumor bulging of inner and outer tables in left temporal bone. **B.** Axial T2WI shows cortical destruction with intracranial and extracranial extension of tumor.

(long bone)
 8.6%가
 (osteoblastic pattern)가 가
 (6). MRI T2 -
 (Fig. 11A, B).
 (Multiple myeloma)
 가 40 - 70
 Bence Jones 가
 가
 (Fig. 12), (punched - out lesions)
 (7).
 X- CT MRI
 (Malignant fibrous histiocytoma)
 80%

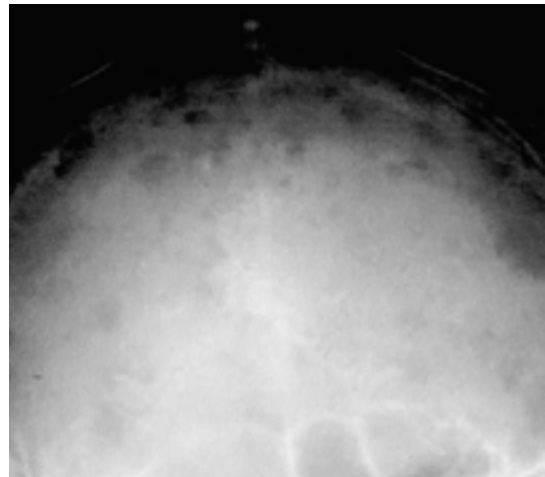


Fig. 12. A 62-year-old male with multiple myeloma. Plain radiograph of skull shows well-defined multiple osteolytic areas scattered throughout the calvarium. Relatively uniform in size and tendency of coalescence are seen.

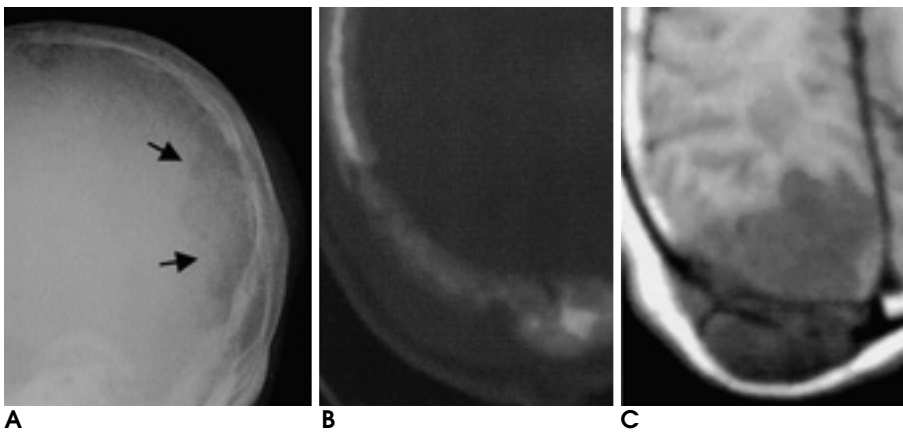


Fig. 13. A 60-year-old male with malignant fibrous histiocytoma.
A. Plain radiograph shows ill-defined osteolytic lesion in right parietal bone (arrows).
B. CT scan shows cortical destruction with a soft tissue mass. There is no periosteal reaction. These findings are not distinguishable from those of fibrosarcoma, lymphoma, and metastasis.
C. T1WI shows cortical destruction with adjacent soft tissue mass. There is homogenous low signal tumor extension to brain parenchyma.

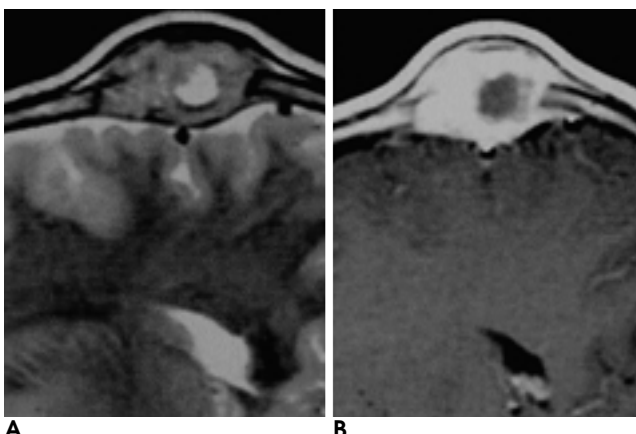


Fig. 14. A 7-year-old female with hemangioendothelioma of the skull.
A. T2WI shows high signal lesion of diploic space with involvement of the inner and outer tables of the skull.
B. Enhanced T1WI shows intense enhancement of tumor.

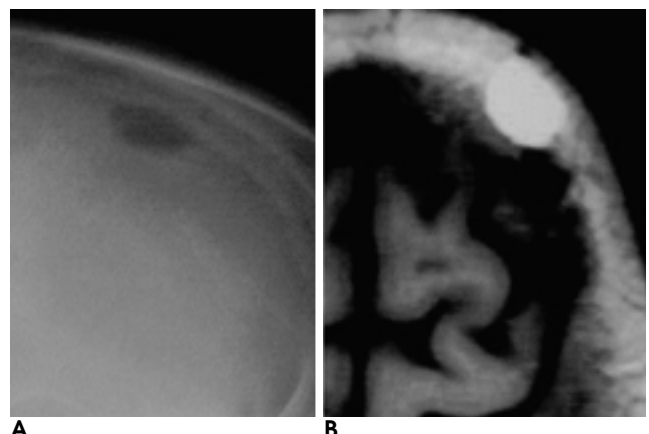


Fig. 15. A 53-year-old female with intraosseous lipoma.
A. Plain radiograph shows a shadow resembling ground glass in the left frontal bone. The margin of mass is sharp, well-circumscribed, but periosteal reaction is not seen.
B. T1WI shows high signal intensity of mass that means adipose tissue in the mass.

(8).

(Fig. 13A, B, C).

(Hemangioendothelioma)

가 2

(9).

가 (diploic

space)

. CT

. MRI

matter)

T1 - (gray

, T2 -

(Fig. 14A).

(Fig. 14B). 가

(Intraosseous lipoma)

가

(Fig.

15A, B).

1. Taveras JM. *Anatomy and examination of the skull*. Hodges FJ. Pathology of the skull. In: Taveras JM, Ferrucci J, EDS. *Radiology: diagnosis, imaging, intervention*, 2nd ed., vol.3. Philadelphia: Lippincott, 1989:1-21
2. Eisenberg RL. *Clinical imaging: an atlas of differential diagnosis*, 2nd ed. Maryland: Aspen publishers, 1992:818-836
3. Arana E, Marti-Bonmati L. CT and MR imaging of focal calvarial lesions. *AJR Am J Roentgenol* 1999;172:1683-1688
4. Thomas J, Baker H. Assessment of roentgenographic lucencies of the skull: a systematic approach. *Neurology* 1975;25:99-106
5. Bastug D, Ortiz O, Schochet SS. Hemangiomas in the calvaria: imaging findings. *AJR Am J Roentgenol* 1995;164:683-687
6. Lee YY, Van Tassel P, Nauert C, Raumont AK, Edeiken J. Craniofacial osteosarcomas: plain film, CT, and MR findings in 46 cases. *AJR Am J Roentgenol* 1988;150:1397-1402
7. Rogers LF, Norris MA. *Bone tumors and related conditions*. In: Juhl JH, Crummy AB, Kuhlman JE. *Essentials of radiologic imaging*, 7th ed., Philadelphia: Lippincott, 1998:158-159
8. Mirra JM, Picci P, Gold RH. *Bone tumors: clinical, radiologic, and pathologic correlations*, vol.2. Beckenham: Lea & Febiger, 1989:766-794, 1087-1117
9. Bourekas EC, Cohen ML, Kamen CS, Tarr RW, Lanzieri CF, Lewin JS. Malignant hemangioendothelioma (angiosarcoma) of the skull: plain film, CT, MR appearance. *AJNR Am J Neuroradiol* 1996;17:1946-1948

Imagings of Skull Vault Lesions¹

Dong Hun Kim, M.D., Choong-Gon Choi, M.D.²

¹Department of Radiology, Armed Forces Kwang Ju Hospital

²Department of Radiology, Asan Medical Center, College of Medicine, University of Ulsan

Lesions of the skull vault are often incidentally encountered during in plain radiography, CT, and MR imaging of the brain and benign lesions are more common than primary malignancies. The usefulness of plain skull films is limited, but when combined with CT or MRI, there is a high probability of accurate diagnosis. The aim of this essay is to describe a wide range of cranial lesions and to illustrate their distinguishing features.

Index words : Skull, radiography
 Skull, CT
 Skull, MR
 Skull, diseases